TRANSPORT PROBLEMS 2025 Volume 20 Issue 1
PROBLEMY TRANSPORTU DOI: 10.20858/tp.2025.20.1.12

Keywords: unmanned ground vehicles; critical components; ballistic protection; simulation

Marek NOWAKOWSKI[1]*, Krzysztof KOSIUCZENKO[2], Jindřich VILIŠ[3]

UNMANNED VEHICLE MOBILITY IMPROVEMENT AGAINST BALLISTIC THREATS DURING SPECIAL MISSIONS: A SIMULATION STUDY

Summary. Implementing unmanned solutions in combat operations transforms battlefield dynamics by minimizing human risks. This study focuses on improving the ballistic protection of key elements in unmanned vehicles to enhance their mobility in hazardous areas. Advancements in unmanned ground vehicle technologies are described. The benefits of developing optionally unmanned vehicles for special purposes are indicated. The high-mobility manned-unmanned TAERO vehicle is introduced, and its structure and parameters are described. Operational limitations arising from potential threats during military missions are identified. Critical components requiring ballistic protection are selected, and the necessary protection levels are defined. Available materials for additional ballistic protection are described in relation to the NATO STANAG 4569 standard, which applies to logistic and light armored vehicles. Numerical analysis was conducted to evaluate the protection of key vehicle components using the lightest composite armors. This study is crucial for validating the effectiveness of the selected composite material and ensuring that its implementation meets the required standards for providing the desired level of ballistic protection for unmanned vehicles. The results confirm that the proposed solution improves the TAERO mobility in dangerous zones.

1. INTRODUCTION

There is a growing demand for unmanned solutions in both commercial and military applications. Integrating these vehicles into combat operations is changing battlefield dynamics and allowing strategic planning and execution of military operations to minimize the exponential risks associated with deploying military forces [1-2].

Special purpose unmanned ground vehicles (UGVs) perform essential tasks that enhance operational efficiency and reduce risks to human soldiers. Key roles include reconnaissance and surveillance, logistics and supply transport, and explosive ordnance disposal (EOD) [3]. UGVs provide combat support by engaging enemy targets and offering force protection with mounted weapon systems. They are crucial in casualty evacuation (CASEVAC) and removing injured personnel from danger zones [3]. These vehicles offer enhanced flexibility and adaptability by seamlessly integrating manned and unmanned operations [4]. Integrating unmanned functionality into already proven structures is an important aspect of advancing unmanned vehicle capabilities. This approach allows vehicles to be quickly reconfigured into unmanned versions when operating in high-risk areas, thereby enhancing operational readiness and response capabilities. The transition between modes based on mission requirements and threat levels significantly boosts personnel safety by executing high-risk tasks

[1] Military Institute of Armoured and Automotive Technology; Okuniewska 1, 05-070 Sulejówek, Poland; e-mail: Marek.Nowakowski@witpis.eu; orcid.org/0000-0003-3864-076X
[2] Military Institute of Armoured and Automotive Technology; Okuniewska 1, 05-070 Sulejówek, Poland; e-mail: Krzysztof.Kosiuczenko@witpis.eu; orcid.org/0000-0002-3097-5488
[3] University of Defence, Faculty of Military Technology, Department of Mechanical Engineering; Kounicova 65, 662 10 Brno, Czech Republic; e-mail: jindrich.vilis@unob.cz; orcid.org/0000-0003-1690-8454
* Corresponding author. E-mail: marek.nowakowski@witpis.eu

remotely and minimizing exposure to danger. These vehicles are equipped with advanced tactical capabilities, improved command and control systems, and cost-effectiveness, making them invaluable assets in modern military operations.

Currently, advancements in unmanned ground vehicles are focused on several key research fields. These include enhancing autonomous navigation capabilities through improved environmental sensing and perception systems such as cameras, lidar, radar, and inertial measurement units (IMUs). Researchers are also developing robust obstacle detection and avoidance technologies to ensure safe traversal of challenging terrains, including rough surfaces and dense vegetation [5-6]. Additionally, research is being carried out to optimize communication reliability between UGVs and command centers, which is essential for real-time data transmission and remote operation.

Despite advancements in control systems, the development of unmanned ground platforms requires careful consideration of potential combat situations in which the vehicles could be exposed to different types of ballistic threats. This issue has gained practical importance, especially considering recent events that reflect real operational scenarios, such as the Field Experimentation Exercise (FEX) 2024 at the Nowa Dęba military training ground. A noteworthy vehicle mobility issue is ballistic resistance, which is essential for effectively conducting logistic missions in threat areas under fire. Such protective measures ensure that unmanned vehicles can continue operating effectively even under hostile conditions, thereby enhancing overall mission resilience and success rates.

This study examines the ballistic resistance of composite armor and its impact on the mobility of the TAERO high-mobility unmanned vehicle. The study quantifies these effects by assessing the ballistic performance of the proposed composite armor through numerical simulations and ballistic testing in accordance with NATO STANAG 4569 Level 1 protection standards (7.62-mm FMJ M80 projectile). This research focuses on the TAERO vehicle, developed by a consortium comprising the Military Institute of Armored and Automotive Technology, STEKOP, AutoPodlasie, and AP Solutions [7]. The results demonstrate the applicability of numerical simulations for evaluating ballistic resistance while providing data on a structural configuration that reduces areal density without compromising Level 1 ballistic protection requirements. These findings contribute to the development of a comprehensive ballistic protection strategy for unmanned ground systems designed for deployment in challenging operational environments.

2. DESCRIPTION OF THE DEVELOPED MANNED–UNMANNED PLATFORM (TAERO)

The operational use of special vehicles in high-risk areas presents significant threats to personnel and requires the consideration of remote execution of these actions. Two primary approaches to unmanned vehicles exist: designing structures from scratch or converting existing, proven models. The second option is currently preferred due to its quicker implementation and ability to expand existing fleets with new options. The TAERO vehicle was developed following this strategy and was specifically designed for both public roads and off-road conditions. It incorporates experience gained from the AERO vehicle, which has been launched to the Polish Armoured Forces. The prototype is designed with a frame structure and a body made from sheet metal, and it does not include armor protection, as shown in Fig. 1.

TAERO operates in manned mode with a driver but can be quickly converted into unmanned mode based on the combat situation and the nature of military or non-military threats [7]. The vehicle is equipped with a central processing unit featuring the IT infrastructure, a precise GPS integrated with an IMU, situational awareness sensors, and mechatronic drives designed to control the platform's factory-fitted mechanisms. A security module handles access authorization and resource management, while high-data-rate radio systems enable the transmission of control and vision signals with minimal delays. The vehicle's architecture supports the integration of additional modules, such as observation heads, weapon systems, and threat detection systems.

A hybrid drive system combines a main diesel engine with an auxiliary electric motor for silent operation. This setup allows for a range of up to 400 km in diesel mode and up to 30 km in electric mode, supported by a 30 kWh battery with an energy recovery system. The vehicle's high off-road capability is ensured by its durable and reliable four-wheel drive system, rigid axles, differential lockers,

and mud-terrain tires with run-flats. The vehicle can achieve a maximum speed of 100 km/h, with a suggested operational speed of 50 km/h. The TAERO has a curb weight of 2,800 kg and a carrying capacity of 1,000 kg, making it well-suited for a variety of specialized missions and tasks. This configuration, proven by the Polish Armed Forces, guarantees robust performance in both manned and unmanned modes across various operational environments.

Fig. 1. View of a TAERO vehicle during operational conditions

The unmanned mode enables remote-controlled driving, autonomous waypoint navigation, and "follow me" mode, allowing the vehicle to support a variety of tasks like reconnaissance and convoy operations. (Fig. 2a).

(a) (b)

Fig. 2. Operational modes of TAERO vehicle: (a) unmanned and (b) manned

Deploying the TAERO platform in real battlefield conditions will require additional ballistic protection to reduce the risk of rapid neutralization by enemy fire, even if the vehicle primarily operates in unmanned mode within high-risk zones. Considering these requirements, a comprehensive analysis of the platform's structural design and material composition is essential to balance ballistic resistance, additional weight, and logistical performance.

3. SELECTION OF TAERO VEHICLE PARTS FOR BALLISTIC PROTECTION

As unmanned ground vehicle technologies develop, new perspectives are arising, but so are new security challenges. A key factor that requires special attention is the protection of these vehicles against ballistic threats [1, 2].

Ballistic protection for autonomous vehicles is a protective device that minimizes the risk of damage to the vehicle or injury to persons after the impact of a ballistic threat, such as projectiles fired from small arms and shrapnel from artillery ammunition. The main requirement for ballistic protection is the ability to provide resistance to these threats while maintaining its minimum areal weight. Increasing weight harms the efficiency and maneuverability of these vehicles, which limits their combat capability.

Regarding the ballistic protection of these vehicles, there is a wide range of critical parts that can be targeted or present a risk to the integrity and functionality of the vehicle. Each aspect of autonomous

vehicles represents an important part of the mosaic of military deployments that requires careful analysis and protection from potential ballistic threats [8].

Sensors are important components of unmanned vehicles in terms of environmental detection and mobility. Sensors such as RADAR, LiDAR, ultrasonic sensors, cameras, Global Navigation Satellite System receivers, accelerometers, and various environmental sensors support autonomus functionality but are challenging to protect effectively with ballistic methods without compromising sensitivity [9-10]. Therefore, redundant systems, like obstacle detection backups, can be utilized to enhance reliability by ensuring continuous operation if primary systems fail.

Propulsion modules, such as electric, hybrid, and internal combustion engines and gearboxes, are crucial for combat functionality and often provide inherent ballistic protection due to their structural placement and connections [11], thereby minimizing the risk of damage.

In relation to the TAERO vehicle's structure, it is crucial to consider the above-mentioned issues. An analysis indicates that the central control system is a crucial component vulnerable to damage in hazardous environments. Although the unmanned system includes redundancy and the drive module is designed to endure harsh conditions (with the engine capable of running for a limited time even with an oil or coolant leak), protecting the central control system has remained important for the successful operation under shelling or hostile fire.

Armoring light vehicles such as TAERO requires a balance to be achieved between increasing protection and maintaining essential functions such as transport and logistics capabilities. Protection must be able to resist 7.62-mm projectiles, and proper analysis is required to identify the critical parts of the vehicle that require protective materials. For this purpose, four key elements have been selected: the control system cover, the two front fenders, and the front grille (Fig 3).

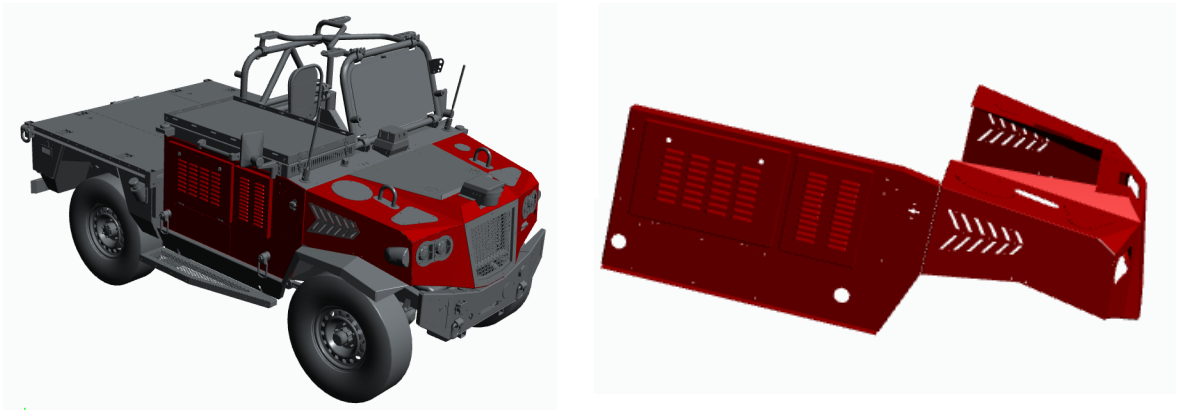

Fig. 3. Selection of crucial components for ballistic protection (parts marked red)

4. PROPOSED MATERIAL AND ITS FEATURES

The design and selection of material for additional ballistic protection are derived from the required level of protection, which is based on the standard NATO STANAG 4569 [12].

The materials used in ballistic protection can be classified into two main categories: metallic and non-metallic [13]. Metallic materials are often used for ballistic protection, including steel, aluminum alloys, and titanium. Steel is one of the oldest and most widely used materials in ballistic protection. The ballistic properties of different steels depend on their hardness, yield strength, tensile strength, toughness, and strain hardening rate. Their main disadvantage is their high density. The most widely used steels are the Swedish low-alloy steels of the Armox® and Hardox® series, the French Mars®, and the Russian TMO77 and 2P. In a previous study, Ranaweera et al. [14] investigated the ballistic resistance of monolithic steel armor and tri-metallic systems using Armox 500T with a thickness of 6 mm as the reference sample. This armor, with an areal weight of 47 kg/m², was able to withstand a 7.62-mm FMJ M80 projectile. The study revealed that the tri-metallic armor—specifically the

combination of 4 mm steel, 1 mm titanium alloy Ti-6Al-4V, and 5.6 mm aluminum alloy Al7075-T651—demonstrated comparable ballistic resistance to the monolithic Armox 500T plate. After normalizing the results based on areal weight, the ballistic limit velocity of this combination was similar to that of the Armox 500T armor.

Composite materials have been implemented in order to reduce the areal weight of ballistic protection and increase ballistic resistance. Composite materials are made of two or more material components. The matrix represents a continuous material component. The discontinuous phase is known as reinforcement. Compared to the matrix, the reinforcement has significantly higher mechanical properties (modulus of elasticity, strength, hardness, etc.) [15, 16]. Currently, the main composite materials for ballistic protection include ballistic-resistant fabrics. The fibers most commonly used for ballistic protection are polymer fibers, namely aramid fibers (aromatic polyamides) and ultra-high molecular weight polyethylene fibers (UHMWPE) [17].

Aramid fibers are synthetically produced fibers made from aromatic polyamides. Their molecular structure consists of long chains of polymers with dimensions on the order of nanometers. The fibers are then spun into yarn, which is used to produce woven textiles. Aramid fibers have high strength and extremely low weight. Another significant advantage of these fibers is their resistance to most chemicals and high temperatures, which makes them suitable for a wide range of applications in various sectors, from protective clothing to structural elements in ballistic protection. Their disadvantages include their tendency to degrade under UV light and their tendency to absorb moisture. The most commonly used aramids for ballistic protection are Kevlar® from DuPont and Twaron® from Teijin [18, 19].

UHMWPE fibers consist of extremely long polyethylene chains that are oriented in one direction. UHMWPE fibers are characterized by a lower density than aramids, a higher tensile modulus, and low elongation at break. They are characterized by high resistance to abrasion and chemicals (except for some oxidizing acids). Their main advantages over aramids are that they do not absorb water and they are UV resistant. Their disadvantages include their relatively low melting point (around 150 °C) and low coefficient of friction. They are used in ballistic protection in the form of flexible UD laminates. The most common UHMWPEs are Dyneema® from DSM and Spectra® from Honeywell [18, 19].

This study aimed to create a numerical model of layered composite ballistic protection with ballistic resistance against rifle cartridges in military caliber 7.62×51 mm NATO FMJ M80 according to STANAG 4569, protection level I. The tested ballistic protection consisted of a Twaron CT 747 para-aramid composite panel with dimensions of 300 × 300 × 32.5 mm and a UHMWPE Endumax Shield XF33 composite panel with dimensions of 300 × 300 × 6.8 mm. The combination of Twaron and Endumax for ballistic protection was chosen primarily based on the objective of reducing areal density while ensuring a high level of protection against 7.62×51 mm NATO FMJ M80 rifle ammunition.

The commercially available materials, Twaron CT 747 and Endumax Shield XF33, were supplied by Teijin Aramid. Twaron CT 747, a para-aramid fabric with a density of 1,440 kg/m³ and a plain weave structure, was used to create the composite panel by stacking 70 layers. Endumax Shield XF33, an ultra-high molecular weight polyethylene with a density of 970 kg/m³ and characterized by an orthogonal asymmetric layer structure [0/90], was used to produce a panel consisting of 40 layers. The Twaron CT 747 LG700 + HG700 composite panel was manufactured using the vacuum assisted resin transfer molding method. The fabric was cut to the required dimensions and placed into a mold. A matrix consisting of epoxy resin LG700 and hardener HG700, mixed in a 100:30 ratio, was then prepared. The fabric impregnation process was carried out under a vacuum. After impregnation, the composite panel was cured at room temperature (23°C) for 24 hours. The Twaron CT 747 ER68 panel was manufactured using autoclave technology. The fabric was pre-impregnated with the thermosetting resin ER68. The panel was cured in the autoclave under the following conditions: the heating rate was set to 3°C/min, the curing temperature reached 120°C, the autoclave chamber pressure during curing was maintained at 5 bar, and the curing time was 60 minutes. After curing, the samples were cooled at a rate of 2°C/min. The Endumax composite panel was fabricated using hot pressing technology. Fabrication was performed using a ZD40 (Brno, Czech Republic) laboratory press at a pressing temperature of 135 ± 2°C and a force of 300 kN for 15 minutes. After pressing, the materials were cooled at a controlled rate of 12°C/min to finalize the composite panels.

The assembled test composite armor consisted of composite panels: Twaron CT 747 LG700 + HG700, Twaron CT 747 ER68, and two panels of Endumax Shield XF33. This protection, composed of a total of 110 layers, had a thickness of 39.3 mm, a weight of 3.3 kg, and an areal weight of 36.7 kg/m². The variant of the composite ballistic protection is shown in Fig. 4.

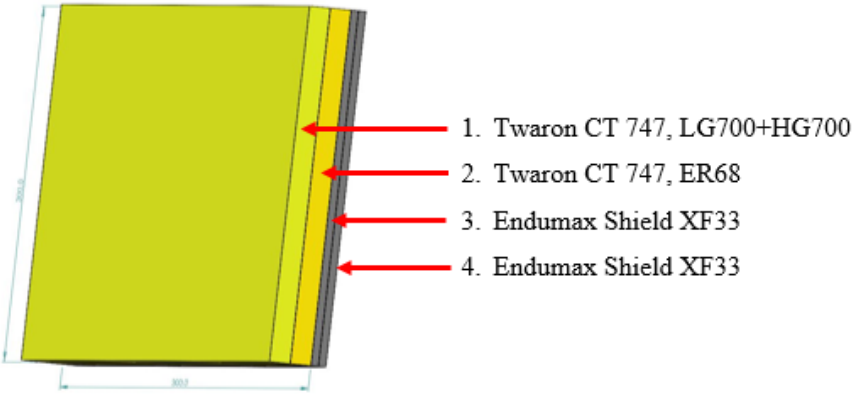

Fig. 4. Construction of the ballistic panel; the test armor had 110 layers and a total thickness of 39.3 mm

5. NUMERICAL SIMULATION OF BALLISTIC PROTECTION METHODS

The impact of a 7.62-mm FMJ M80 projectile on composite armor (Twaron/Endumax) was numerically analyzed. The 7.62-mm FMJ M80 projectile was discretized into 9,071 hexahedral elements, each with eight nodes (using the 10-node format in LS-DYNA). The mesh was refined near the projectile's tip with elements sized at 0.1 mm. Fig. 5 shows the FE model of the 7.62-mm FMJ M80 projectile, along with a detailed description of its components.

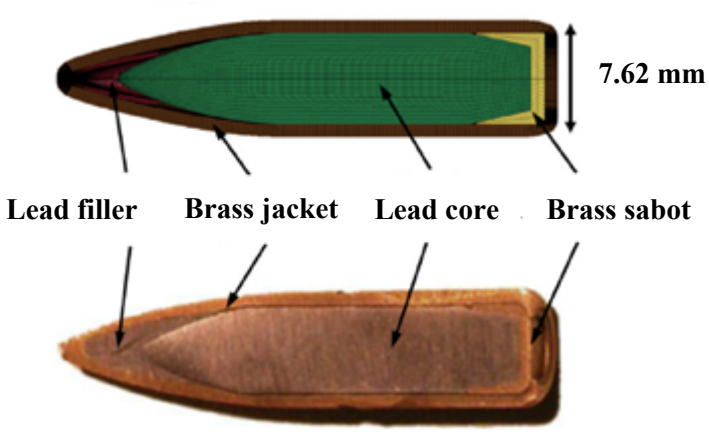

Fig. 5. Cross-section of the 7.62-mm FMJ M80 projectile

The parameters of the projectile and the composite armor materials used in the model are summarized in Tables 1 and 2. The analysis was carried out to show the initiation of damage to the panels, the courses of energy absorption, the instantaneous velocity of the projectile, and the penetration of the laminate by the projectile. For this purpose, the finite element method, implemented in the LS DYNA computational program [20], was used. This program is specifically designed for the numerical simulation of the rapid and extreme materials deformation response of structures. The FE model was created using 2D shell elements to represent the laminate and 3D solid elements to represent the projectile, as shown in Figs. 6 and 7.

The SHELL elements use the Belytschko-Tsay option (ELFORM=2), which is optimal for modeling composites in LS-DYNA with *PART_COMPOSITE, as it combines high computational efficiency (one integration point through element thickness) with good accuracy. It is compatible with the

*PART_COMPOSITE definition, which manages integration points through laminate thickness independently, ensuring numerical stability in dynamic simulations.

Table 1

Material parameters of the composite armor

Name	Twaron CT747	Endumax Shield XF33
MAT (model)	_22	_22
RO (density)	1,450 kg/m³	970 kg/m³
EA (Young's modulus)	115 GPa	170
EB (Young's modulus)	5 GPa	7 GPa
PRBA (Poisson's ratio)	0.2	0.2
GAB (shear modulus)	24.4 GPa	4.5 GPa
SC (shear strength)	1.1 GPa	0.35 GPa
XT (tensile strength)	4.8 GPa	4.0 GPa
YT (transverse tensile strength)	4.8 GPa	4.0 GPa
YC (transverse compressive strength)	1.2 GPa	0.7 GPa

Table 2

Material parameters of the 7.62-mm FMJ M80 projectile (core, jacket, and filler)

Names	Core-Lead	Jacket-Brass	Filler-Lead
MAT (model)	_024	_024	_024
RO (density)	11,340 kg/m³	8,200 kg/m³	11,340 kg/m³
E (Young's modulus)	16 GPa	115 GPa	16 GPa
PR (Poisson's ratio)	0.46	0.42	0.46
SIGY (Yield stress)	200 MPa	200 MPa	200 MPa
ETAN (tangent modulus)	0	0	0
FAIL (failure strain)	0.9	0.9	0.9

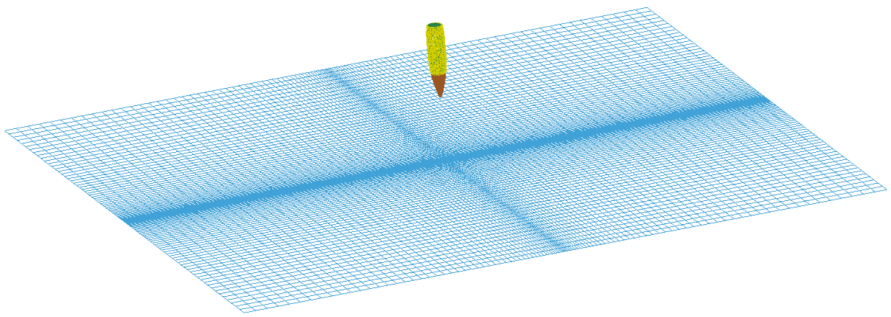

Fig. 6. SHELL flat finite element mesh of 0.2 mm to 4 mm mapping of the composite (use of BIAS density from the edge to its center)

The density of the finite element mesh was preceded by an analysis of the model's sensitivity to element size. Four-quadrant panels with a thickness of 39.3 mm were analyzed, in which the individual material layers (Twaron-Twaron-Endumax-Endumax) had thicknesses of 0.50, 0.40, 0.17, and 0.18 mm, respectively. Each layer of material was a multilayer composite with the 35 layers for the first two groups and 20 layers for remain groups. The panel was restrained at its perimeter, while the projectile was given an initial velocity of 833 m/s. A general view of the developed model is shown in Fig. 8.

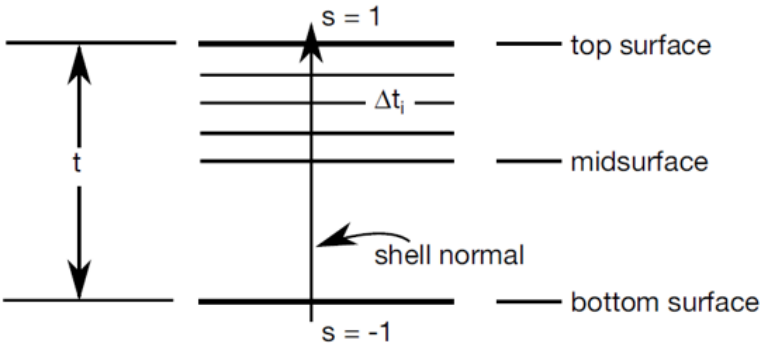

Fig. 7. Zoomed-in physical cross-section of each layer of the SHELL element (shown in Fig. 4)

The finite element method (FEM) model used data provided by the experiment from the Defense University (Brno, Czech Republic). Due to the limited range of data provided, an orthotropic material model was used to model the composite, including failure criteria: MAT_022 (COMPOSITE_DAMAGE) [20]. The use of SHELL elements was dictated both by the reduction in computation time and the possibility of using laminated shell theory (LST).

Spatial distributions of stress, deformation, and failure within the composite armor and projectile structures were obtained as a result of numerical calculations performed on a multiprocessor computing cluster. The deformations of the projectile in the subsequent moments proceeded as shown in Fig. 9. The time course of the projectile's velocity loss is shown in Fig. 10.

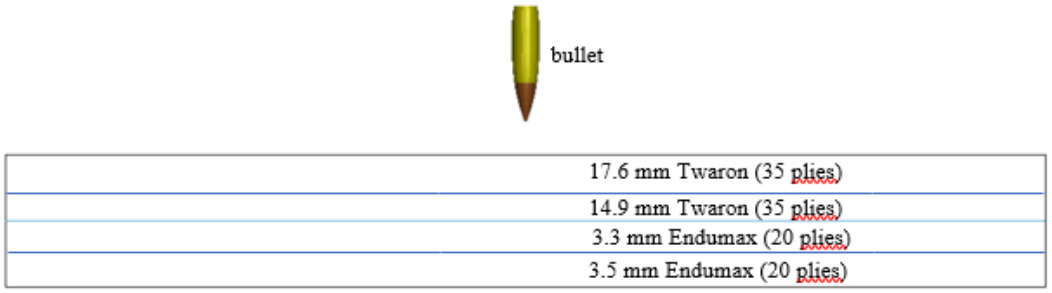

Fig. 8. A general view of the model

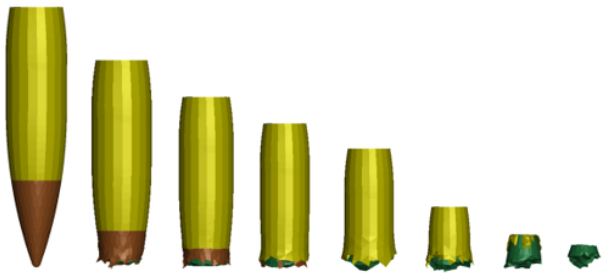

Fig. 9. The deformations of the projectile in the subsequent moments

Numerical simulations have revealed that the penetration behavior of the 7.62-mm FMJ M80 projectile is predominantly governed by the mechanical properties of the lead-antimony alloy core. The contribution of the tombac jacket to the penetration process is minimal, primarily affecting the kinetic energy transfer rather than the overall penetration depth. The calculated penetration depth of the composite armor, as shown in Fig. 11, slightly exceeded half of its thickness, which contrasts with the experimental observations. This deviation could be attributed to the use of conservative material properties for the composite or the overestimation of the strength characteristics of the lead-antimony alloy core in the numerical model.

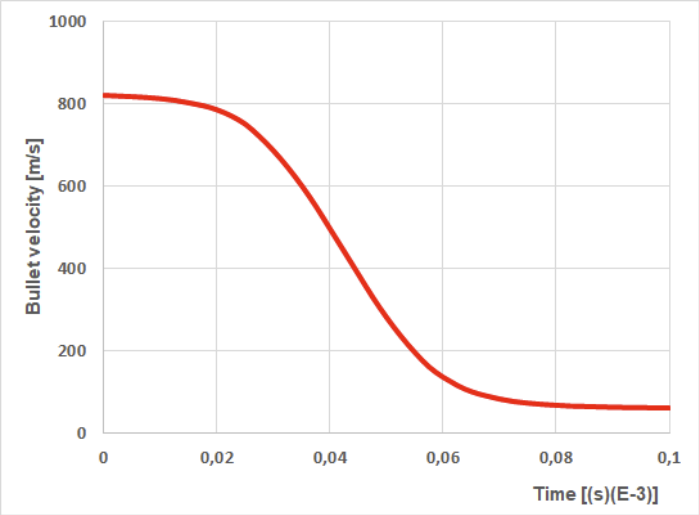

Fig. 10. The time course of the projectile's velocity loss

Deformations of the top and bottom layers of the composite by the projectile are shown in Fig. 11. Additionally, during the simulation process, composite materials were modeled using single SHELL plane elements. Each of these elements had a defined layer structure, with numerical calculations performed for each layer. Due to the large number of layers (110), by default, only three layers (TOP, MID, and BOTTOM) are shown in Fig 12. This amount of information is generally sufficient for strength design, though it can be extended. Although storing data for all layers is possible, it would require significantly more data storage resources.

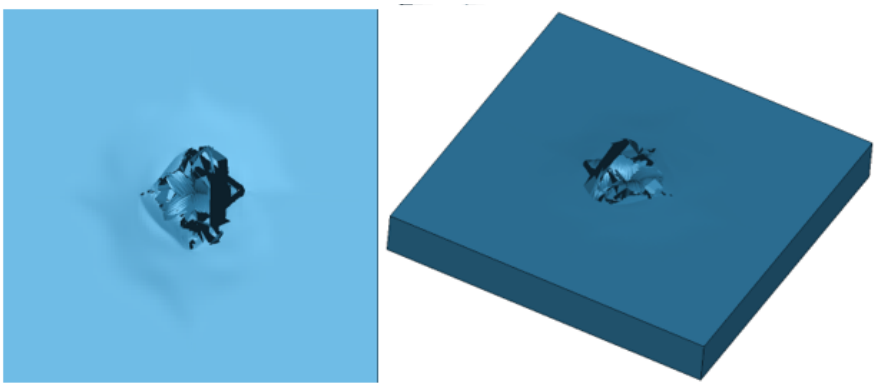

Fig. 11. View of the damaged composite armor from the outlet side

The stress maps show scalar equivalent von Mises stress values and are presented according to the local Z direction of the SHELL element, illustrating the stress state in successive layers of this element (from BOTTOM to TOP). Differences in stress distribution across layers result from varying projectile penetration depths and the different fiber orientations in each layer. Each layer has a unique fiber orientation defined by angle β (b1, b2, etc.) and is constructed from either Twaron CT747 or Endumax XF33 material. The above analysis helps identify stress concentrations and how effectively each layer absorbs and redistributes impact forces. This comprehensive understanding aids in improving the overall design and material performance of composite structures.

Considering the numerical simulation results, ballistic tests were also conducted in the laboratory of the Defense University to validate the numerical outcomes. These tests aimed to verify the accuracy of the penetration behavior, damage initiation, and energy absorption processes observed in the computational models. Fig. 13 shows the high-speed camera (Photron, SA-Z, Japan) recording of the impact of the 7.62-mm FMJ M80 projectile on the designed composite ballistic protection.

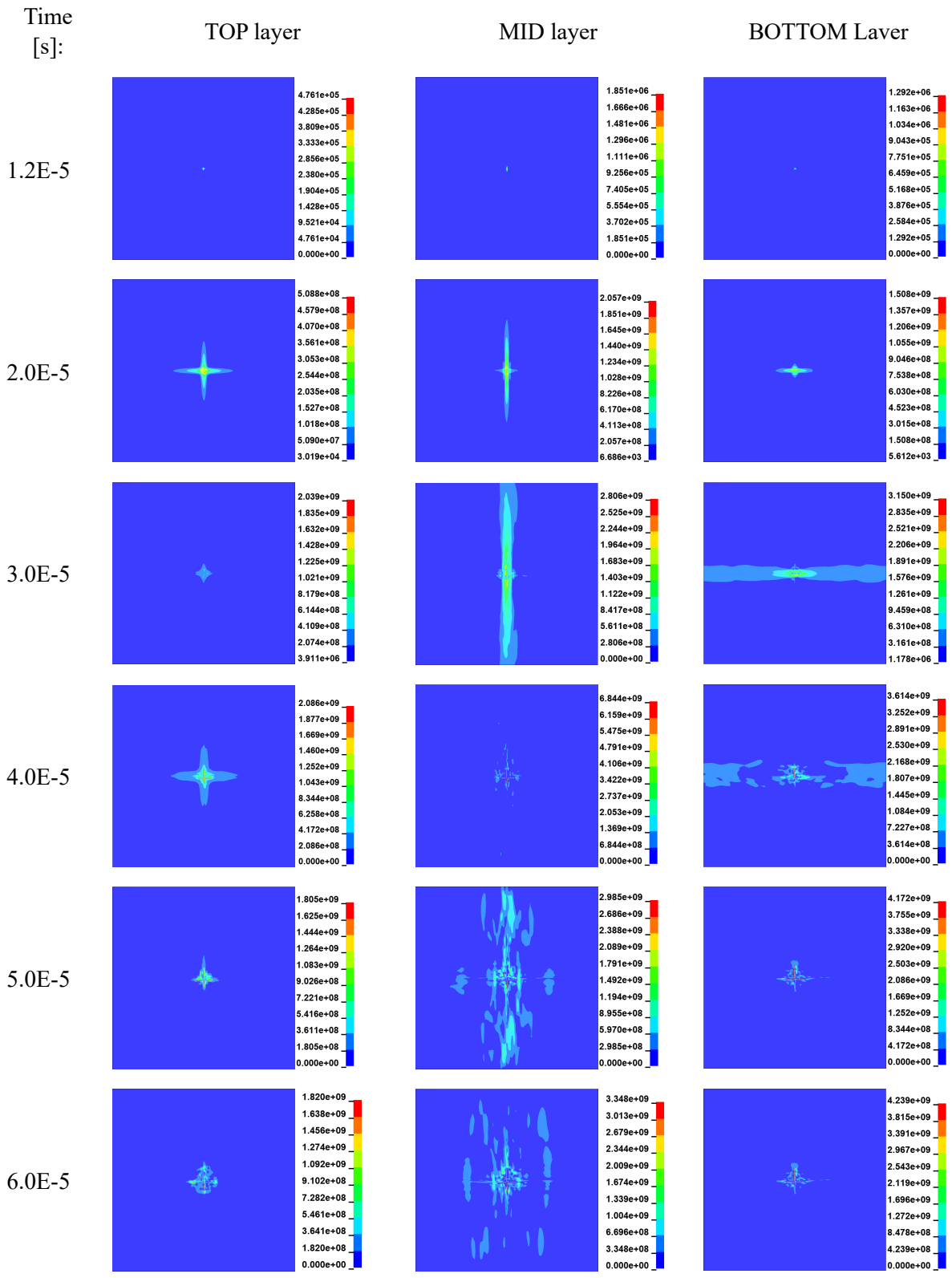
Time [s]:
TOP layer
MID layer
BOTTOM Laver
1.2E-5
4.761e+05
4.285e+05
3.809e+05
3.333e+05
2.856e+05
2.380e+05
1.904e+05
1.428e+05
9.521e+04
4.761e+04
0.000e+00
1.851e+06
1.666e+06
1.481e+06
1.296e+06
1.111e+06
9.256e+05
7.405e+05
5.554e+05
3.702e+05
1.851e+05
0.000e+00
1.292e+06
1.163e+06
1.034e+06
9.043e+05
7.751e+05
6.459e+05
5.168e+05
3.876e+05
2.584e+05
1.292e+05
0.000e+00
2.0E-5
5.088e+08
4.579e+08
4.070e+08
3.561e+08
3.053e+08
2.544e+08
2.035e+08
1.527e+08
1.018e+08
5.090e+07
3.019e+04
2.057e+09
1.851e+09
1.645e+09
1.440e+09
1.234e+09
1.028e+09
8.226e+08
6.170e+08
4.113e+08
2.057e+08
6.686e+03
1.508e+09
1.357e+09
1.206e+09
1.055e+09
9.046e+08
7.538e+08
6.030e+08
4.523e+08
3.015e+08
1.508e+08
5.612e+03
3.0E-5
2.039e+09
1.835e+09
1.632e+09
1.428e+09
1.225e+09
1.021e+09
8.179e+08
6.144e+08
4.109e+08
2.074e+08
3.911e+06
2.806e+09
2.525e+09
2.244e+09
1.964e+09
1.683e+09
1.403e+09
1.122e+09
8.417e+08
5.611e+08
2.806e+08
0.000e+00
3.150e+09
2.835e+09
2.521e+09
2.206e+09
1.891e+09
1.576e+09
1.261e+09
9.459e+08
6.310e+08
3.161e+08
1.178e+06
4.0E-5
2.086e+09
1.877e+09
1.669e+09
1.460e+09
1.252e+09
1.043e+09
8.344e+08
6.258e+08
4.172e+08
2.086e+08
0.000e+00
6.844e+09
6.159e+09
5.475e+09
4.791e+09
4.106e+09
3.422e+09
2.737e+09
2.053e+09
1.369e+09
6.844e+08
0.000e+00
3.614e+09
3.252e+09
2.891e+09
2.530e+09
2.168e+09
1.807e+09
1.445e+09
1.084e+09
7.227e+08
3.614e+08
0.000e+00
5.0E-5
1.805e+09
1.625e+09
1.444e+09
1.264e+09
1.083e+09
9.026e+08
7.221e+08
5.416e+08
3.611e+08
1.805e+08
0.000e+00
2.985e+09
2.686e+09
2.388e+09
2.089e+09
1.791e+09
1.492e+09
1.194e+09
8.955e+08
5.970e+08
2.985e+08
0.000e+00
4.172e+09
3.755e+09
3.338e+09
2.920e+09
2.503e+09
2.086e+09
1.669e+09
1.252e+09
8.344e+08
4.172e+08
0.000e+00
6.0E-5
1.820e+09
1.638e+09
1.456e+09
1.274e+09
1.092e+09
9.102e+08
7.282e+08
5.461e+08
3.641e+08
1.820e+08
0.000e+00
3.348e+09
3.013e+09
2.679e+09
2.344e+09
2.009e+09
1.674e+09
1.339e+09
1.004e+09
6.696e+08
3.348e+08
0.000e+00
4.239e+09
3.815e+09
3.391e+09
2.967e+09
2.543e+09
2.119e+09
1.696e+09
1.272e+09
8.478e+08
4.239e+08
0.000e+00

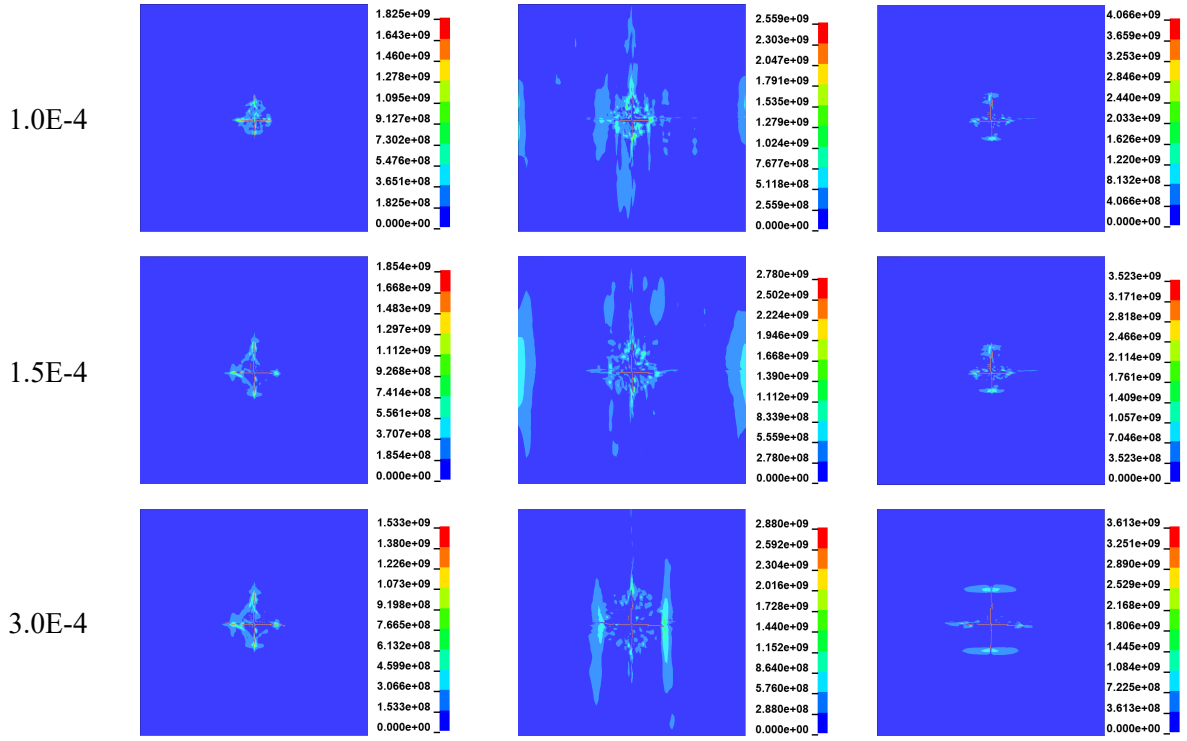

Fig. 12. Distributions of reduced stresses (von Mises criterion) in successive punching phases in the top (TOP), bottom (BOTTOM) and middle (MIDDLE) layers

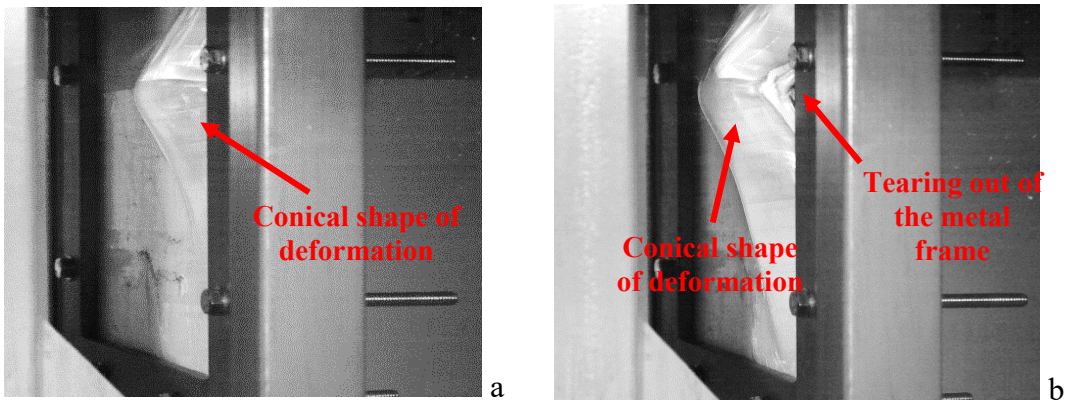

Fig. 13. Photos from the high-speed camera: gradual plastic deformation of the layered composite armor

The deformation and destruction of the composite armor material observed in the simulation closely matched those observed during the experiment (Fig. 12). The conical deformation observed on the posterior side of the composite armor following projectile impact manifested as a funnel-shaped indentation. The observed failure mechanism of the composite armor involved the initial stretching and subsequent tearing of the primary fibers, followed by delamination of the matrix. This progression ultimately led to the shear rupture of the fibers.

6. CONCLUSIONS

This study focused on material selection, numerical simulations, and ballistic resistance evaluation for the development of ballistic protection for the TAERO autonomous vehicle, designed for operations

in high-risk areas. The study aimed to test layered ballistic protection with an areal weight of 36.7 kg/m² against a 7.62-mm FMJ M80 projectile. Composite materials such as Twaron CT 747 and Endumax Shield XF33 were selected. The material selection for ballistic protection was based on ensuring the required ballistic resistance while minimizing the vehicle's areal weight, which is crucial for maintaining maneuverability and operational capabilities.

Numerical simulations conducted using the FEM were a key tool for optimizing the design of the ballistic protection. The simulations allowed for a detailed analysis of material behavior under ballistic impact, focusing on stress distribution, deformation, and energy absorption capabilities of individual panels. Experimental ballistic testing was also conducted following the NATO STANAG 4569 standard. The ballistic tests confirmed the validity of the numerical models. The results of the simulations and tests demonstrated that the tested ballistic protection met the required ballistic resistance standards and was not perforated by the 7.62-mm FMJ M80 projectile.

The results indicate that the use of composite materials, as opposed to conventional Armox 500T steel plates, reduces the areal density of ballistic protection by approximately 22%, as presented in Chapter 4 of the study by Ranaweera et al. [14].

Acknowledgments

The paper is a part of the research under carried out project no. 55.23615.PR at the Military Institute of Armoured and Automotive Technology. The work was also supported by the specific research project "SV23-216" at the Department of Mechanical Engineering, University of Defence in Brno, and was supported by the Project for the Development of the Organization "VAROPS (DZRO VAROPS) Military autonomous and robotic assets" by the Ministry of Defence of Czech Republic.

This research was carried out with the support of the Interdisciplinary Centre for Mathematical and Computational Modelling at the University of Warsaw (ICM UW).

References

1. National Research Council. *Technology Development for Army Unmanned Ground Vehicles.* Washington, DC: The National Academies Press. 2002. ISBN 978-0-309-08620-2. DOI: 10.17226/10592.
2. Whitson, J.A. & Gorsich, D. & Vantsevich, V.V. & Letherwood, M. & Sapunkov, O. & Moradi, L. Military unmanned ground vehicle maneuver: a review and formulation. *SAE Technical Paper*. 2023. DOI: 10.4271/2023-01-0108.
3. Swett, B.A. & Hahn, E.N. & Llorens, A.J. Designing robots for the battlefield: State of the art. *Robotics, AI, and Humanity: Science, Ethics, and Policy*. 2021. P. 131-146. DOI: 10.1007/978-3-030-54173-6_11.
4. Giurgiu, T. & Virca, I. & Grigoraș, C. & Năstăsescu, V. Trends in development of military vehicles capabilities based on advanced technologies. In: *International conference Knowledge-Based Organization.* 2023. Vol. 29. No. 3. P. 15-22.
5. Konecny, V. & Jaśkiewicz, M. & Downs, S. Motion planning and object recognition algorithms, vehicle navigation and collision avoidance technologies, and geospatial data visualization in network connectivity systems. *Contemporary Readings in Law and Social Justice*. 2022. Vol. 14(1). P. 89-104. DOI: 10.22381/CRLSJ14120226.
6. Beycimen, S. & Ignatyev, D. & Zolotas, A. A comprehensive survey of unmanned ground vehicle terrain traversability for unstructured environments and sensor technology insights, *Engineering Science and Technology*. 2023. Vol. 47. No. 101457. DOI: 10.1016/j.jestch.2023.101457.
7. Nowakowski, M. & Berger, G.S. & Braun, J. & Mendes, J.A. & Bonzatto Junior, L. & Lima, J. Advance reconnaissance of UGV path planning using unmanned aerial vehicle to carry our mission in unknown environment. In: Marques, L. & Santos, C. & Lima, J.L. & Tardioli, D. & Ferre, M.

(eds). *Robot 2023: Sixth Iberian Robotics Conference. ROBOT 2023. Lecture Notes in Networks and Systems*. 2024. Vol. 978. Springer, Cham. DOI: 10.1007/978-3-031-59167-9_5.
8. Vala, M. & Žalud, Z & Neumann, V. *Teorie a konstrukce bojových a speciálních vozidel: učebnice*. Brno: Univerzita obrany v Brně. 2017. ISBN 978-80-7582-023-5. [In Czech: *Theory and construction of combat and special vehicles*. Textbook].
9. Alinezhad, E. & Gan, V. & Chang, V.W.-C. & Zhou, J. Unmanned ground vehicles (UGVs)-based mobile sensing for Indoor Environmental Quality (IEQ) monitoring: Current challenges and future directions. *Journal of Building Engineering*. 2024. Vol. 88. DOI: 10.1016/j.jobe.2024.109169.
10. Sukop, M. & Grytsiv, M. & Jánoš, R. & Semjon, J. Simple ultrasonic-based localization system for mobile robots. *Applied Sciences.* 2024. Vol. 14(9). No. 3625.
11. Grzejda, R. Determination of bolt forces and normal contact pressure between elements in the system with many bolts for its assembly conditions, *Advances in Science and Technology Research Journal.* 2019. Vol. 13(1). P. 116-121. DOI: 10.12913/22998624/104657.
12. AEP-55 STANAG 4569. *Protection Levels for Occupants of Logistic and Light Armored Vehicles. Part 1-4: General-Annex A. First Edition*. NATO: Brussels. Belgium. 2005. Vol. 1.
13. Acar, D. & Canpolat, B.H. & Cora, Ö.N. Ballistic performances of Ramor 500, Armox Advance and Hardox 450 steels under monolithic, double-layered, and perforated conditions. *Engineering Science and Technology, an International Journal*. 2024. Vol. 51. No. 101653. DOI: 10.1016/j.jestch.2024.101653.
14. Ranaweera, P. & Bambach, M.R. & Weerasinghe, D. & Mohotti, D. Ballistic impact response of monolithic steel and tri-metallic steel–titanium–aluminium armour to nonrigid NATO FMJ M80 projectiles. *Thin-Walled Structures*. 2023. Vol. 182. No. 110200. DOI: 10.1016/j.tws.2022.110200.
15. Campbell, F.C. *Structural Composite Materials*. ASM International. 2010. ISBN 978-1-62708-314-0. DOI: 10.31399/asm.tb.scm.9781627083140.
16. Chen, X. *Advanced fibrous composite materials for ballistic protection*. Woodhead Publishing series in composites science and engineering. UK: Cambridge. 2016. ISBN 978-1-78242-461-1.
17. Crouch, I.G. Body armour – New materials, new systems. *Defence Technology*. 2019. Vol. 15. No. 3. P. 241-253. ISSN 22149147. DOI: 10.1016/j.dt.2019.02.002.
18. *Twaron CT 747. Teijin Limited. Ballistic Materials Handbook*. Japan: Tokyo, Osaka. Available at: https://www.teijinaramid.com/sites/default/files/2023-07/Twaron%20Fabric%20WRT%20-%20ComForte%20-%20%28Prepreg%29%20CT%20TA00109%20Engl.pdf.
19. *Endumax Shield XF33. Teijin Limited. Ballistic Materials Handbook*. Japan: Tokyo, Osaka. Available at: https://www.teijinaramid.com/sites/default/files/2023-07/Endumax-Film-Shield-Fabric-Panel-Laminate-TA00113-English-20210521.pdf.
20. *LSTC, LS-DYNA. Theory manual*. Livermore Software Technology Corporation. 2019.

Received 12.10.2023; accepted in revised form 12.03.2025